

SYSTEM IDENTIFICATION OF A SPHERICAL AIR-BEARING SPACECRAFT SIMULATOR

Jana L. Schwartz[†] and Christopher D. Hall[‡]

The Distributed Spacecraft Attitude Control System Simulator is a testbed comprised of two independent spherical air-bearing platforms, useful for formation-flying attitude control simulation. The DSACSS is intended to support a wide range of functions. As such, requiring that all controllers be robust to approximations of the system parameters is impractical. We document the development of batch system identification techniques for the full, nonlinear equations of motion of the system. We compare the performance of these techniques in several simulations and provide the results obtained from their application on the experimental system.

INTRODUCTION

For many applications, high-precision knowledge of the mass properties of a system is not required. Alternatively, it may be more practical to accept the loss in performance from freezing the model of a system to a set of inaccurate parameters rather than taking the risk of adjusting these terms during a mission and causing potentially unpredictable changes. For such cases — both the low-cost and the high-risk — a simple batch estimation technique for parameter determination is ideal. When maximizing performance is crucial, the computational costs and potential risks associated with an on-line, adaptive estimation scheme become acceptable.

Most modern aerospace engineering design efforts begin within the framework of a computer-assisted drawing (CAD) program. Many CAD programs can be used to compute estimates of the model's mass properties. Such system models can be extremely high resolution: for example, many programs include libraries of fasteners and commonly used commercial parts that are easy to incorporate. However, commercial components are typically drawn as volume models with uniform density. Moreover, flexible items including thruster air harnessing and bus wire harnessing can be prohibitively complex to model, yet quite massive. Particularly in less formal engineering environments (such as those in university settings) production-time design changes may not be reflected in the CAD model. Therefore, the mass properties estimate from a CAD model can be considered a useful tool and an accurate starting place for analysis, but may require substantial improvement.

A reasonable first step for parameter estimation is to use the mass properties from a CAD model to initialize a filter for basic state estimation. The subsequent smoothed attitude and/or rate data can then be used as the inputs for a batch estimation technique such as least-squares estimation (LSE). Such schemes have been used successfully for the air-bearing spacecraft simulators at Georgia Tech¹ and the Air Force Institute of Technology.²⁻⁴ Improvements in batch estimation effectiveness and efficiency are possible through careful choice of the input signal used to excite to the system. Such advanced batch techniques have been used for the Naval Postgraduate School's air-bearing system,⁵

[†]National Science Foundation Fellow, NASA Graduate Student Researcher Program Fellow. Department of Aerospace & Ocean Engineering, Virginia Polytechnic Institute & State University, Blacksburg, Virginia 24061. jana@vt.edu. Student Member AIAA, Student Member AAS.

[‡]Professor. Department of Aerospace & Ocean Engineering, Virginia Polytechnic Institute & State University, Blacksburg, Virginia 24061. cdhall@vt.edu. Associate Fellow AIAA, Member AAS.
Copyright ©2004 by the authors. Permission to publish granted to The American Astronautical Society.

as well as for simulated and flight-data analysis of several spacecraft.⁶⁻¹¹ The literature on batch estimation techniques extends far beyond simple LSE, but this technique serves as a reasonable initial effort for this investigation.

Adaptive, or sequential, techniques vary widely. Adjustments can be made within the observer or the controller algorithm for the system. There are two possible techniques for estimating the parameters of a system within the observer step in a classical Kalman Filter context: dual- and joint-filtering.¹² A joint filter estimates the states and parameters simultaneously, within a single nonlinear Kalman Filter. A dual filter intertwines two filters, one for state estimation and a second for parameter estimation. We have investigated multiple techniques in this area.¹³

In this paper, we document the development and application of batch system identification techniques for an air-bearing spacecraft simulator. We begin with an introduction of Virginia Tech's Distributed Spacecraft Attitude Control System Simulator (DSACSS) and its functionality. We present the equations of motion for the system and demonstrate the parameter dependencies therein. We document the initial estimate for the parameters obtained from a CAD model and derive several candidate LSE techniques that could be used to refine this estimate. The usefulness of each of these techniques is demonstrated through simulation of an ideal system. We identify possible sources of error in the experimental system and increment the realism of the simulation in an effort to predict the accuracy of the experimental results.

EXPERIMENTAL SYSTEM

Virginia Tech has developed a Distributed Spacecraft Attitude Control System Simulator (DSACSS), which includes two independent spherical air-bearing platforms for formation-flying attitude control simulation. Both systems are Space Electronics, Incorporated, models: the smaller is a tabletop-style bearing that can support a 300 lb payload, shown in the foreground of Figure 1. This system, Whorl-I, can tilt $\pm 5^\circ$ from the horizontal and spin freely about the vertical (yaw) axis. Whorl-II is a dumbbell-style bearing (in the background of Figure 1) that can support a 375 lb payload. It provides full freedom in both roll (about the longitudinal shaft axis) and yaw, with $\pm 30^\circ$ of freedom about the pitch axis. Each air bearing is equipped with three-axis accelerometers and rate gyros for attitude determination. Attitude control options include three-axis momentum/reaction wheels, compressed air thrusters, and control moment gyros (CMGs). The payload's center of gravity is maintained at the bearing's center of rotation via a triad of linear actuators; alternatively, attitude control schemes by center of gravity placement can be investigated.

The uniqueness of this system stems not from particular individual capabilities of either platform, but rather the ability to implement distributed control laws between the two. Coupled with a third, stationary system, the DSACSS provides an experimental facility for formation flying attitude control simulation. In contrast, planar test facilities provide a motion base for testing control schemes involving the relative position and relative motion between two bodies, but coordination in pointing is difficult to replicate. The DSACSS testbed allows implementation of algorithms for relative attitude control.¹⁴ Either of the two DSACSS air bearings can also be used independently for specialized investigations of topics in the field of spacecraft attitude dynamics and control.

At the core of each of the DSACSS platforms is a PC/104+ form-factor computer. Each computer includes a 32-bit 133MHz Tri-M MZ104+ ZF86 processor with 64MB of RAM. The operating system (a lean, customized version of Slackware Linux) and command software is stored on a 288MB DiskOnChip solid-state memory device. Operational software is written in C++ with lower level software written in C for reasons of efficiency. Due to the relatively slow clock speed of the computers, computation time is an operational constraint. As such, we do not want to load the processor with unnecessarily complex algorithms; we seek a balance between accuracy and computation time for effective state estimation. For the purposes of this work, much of the computation was performed offline on a more robust system.



Figure 1: Virginia Tech's Distributed Spacecraft Attitude Control System Simulator

The operational code and additional simulation tools for DSACSS laboratory work are maintained in a pair of open source software projects freely available for use. All DSACSS operational code, including filters and controllers, are contained in the DSACSS-Ops project. A diverse collection of simulation tools for both orbital and attitude dynamics are housed in an Open Source, Extensible Spacecraft Simulation and Modeling Environment Framework, Open-SESSAME.^{15,16} The purpose of these software projects is to provide a development framework both for simulation and operation that is easy to use, maintain, and expand.[§]

EQUATIONS OF MOTION

Accurate system identification of both the state vector of attitude quaternions and body angular velocities, along with the nine-term parameter vector (the six unique elements of the moment of inertia matrix along with the three components of the center-of-gravity vector)

$$\mathbf{\Pi} = \{I_{xx}, I_{xy}, I_{xz}, I_{yy}, I_{yz}, I_{zz}, mg r_{gx}, mg r_{gy}, mg r_{gz}\}^T \quad (1)$$

is crucial for successful operation of the DSACSS. We begin by modeling the system as a gyrostat, with all terms written with respect to an inertial, lab-fixed reference frame.

$$\dot{\mathbf{q}} = \mathbf{Q}(\mathbf{q}) \boldsymbol{\omega}_b \quad (2)$$

$$\dot{\mathbf{h}}_b = \mathbf{h}_b^\times \boldsymbol{\omega}_b - mg \mathbf{r}_g^\times \mathbf{R}^{bi} \hat{\mathbf{k}} + \mathbf{g}_{external} \quad (3)$$

$$\dot{\mathbf{h}}_a = \mathbf{g}_a \quad (4)$$

The attitude of the body is represented by the quaternion \mathbf{q} and the rotation matrix \mathbf{R}^{bi} . Body angular velocity and angular momentum are $\boldsymbol{\omega}_b$ and \mathbf{h}_b , respectively. The axial angular momentum

[§]Please see <http://dsacss.sourceforge.net> and <http://spacecraft.sourceforge.net> for additional information on the open source software projects.

of the wheel is \mathbf{h}_a , and the motor torque is \mathbf{g}_a . The gravity gradient torque is due to the offset of the payload's center of mass from the air bearing's center of rotation. All other external forces are contained in $\mathbf{g}_{external}$.

The angular momenta and angular velocities are related by

$$\mathbf{h}_b = \mathbf{I}_b \boldsymbol{\omega}_b + \mathbf{A} \mathbf{I}_s \boldsymbol{\omega}_s \quad (5)$$

$$\mathbf{h}_a = \mathbf{I}_s \mathbf{A}^\top \boldsymbol{\omega}_b + \mathbf{I}_s \boldsymbol{\omega}_s \quad (6)$$

$$\boldsymbol{\omega}_b = \mathbf{J}^{-1} (\mathbf{h}_b - \mathbf{A} \mathbf{h}_a) \quad (7)$$

Note the inertia-like matrix

$$\mathbf{J} = \mathbf{I}_b - \mathbf{A} \mathbf{I}_s \mathbf{A}^\top \quad (8)$$

that is composed of the frozen inertia matrix of the complete rigid body, as above, less the axial moments of inertia of the flywheels. The $3 \times n$ matrix \mathbf{A} defines the axial alignment of each flywheel. The matrix \mathbf{I}_s is a diagonal matrix of the axial moments of inertia of the wheels. We consider this value to be well-known; this approximation is reasonable, as the DSACSS flywheels, although custom made, are simple in design and therefore have easily calculated mass properties.

In order to show that a linear least squares formulation is applicable to the problem we must first demonstrate that the system is linear with respect to the parameters. Note that the parameter vector does not enter into the kinematic equation. However, the attitude of the system is coupled into the solution of the parameters due to the gravity gradient torque in Equation 3. Attitude knowledge is typically not needed for the solution of a torque-free gyostat rotating about its center of mass.

We begin with consideration of the simpler problem formulation of a rigid body. This restatement of the problem, although not applicable in the final solution, is a cleaner statement of the equations. We restore the cross-coupling gyostat terms in the derivation later. The dynamics of a rigid body are governed by

$$\dot{\boldsymbol{\omega}}_b = \mathbf{I}_b^{-1} \left(-\boldsymbol{\omega}_b \times \mathbf{I}_b \boldsymbol{\omega}_b - mg \mathbf{r}_g \times \mathbf{R}^{bi} \hat{\mathbf{k}} + \mathbf{g}_{rigidbody} \right) \quad (9)$$

Grouping the control torques, the dynamics can be written in such a way that the system is clearly linear with respect to the parameters:

$$\mathbf{g}_{rigidbody} = \mathbf{I}_b \dot{\boldsymbol{\omega}}_b + \boldsymbol{\omega}_b \times \mathbf{I}_b \boldsymbol{\omega}_b + mg \mathbf{r}_g \times \mathbf{R}^{bi} \hat{\mathbf{k}} \quad (10a)$$

$$= [\dot{\boldsymbol{\omega}}_b] \{ \mathbf{I}_b \} + [\boldsymbol{\omega}_b^2] \{ \mathbf{I}_b \} + [\mathbf{q}^2] \{ mg \mathbf{r}_g \} \quad (10b)$$

$$= \left[\left([\dot{\boldsymbol{\omega}}] + [\boldsymbol{\omega}^2] \right), [\mathbf{q}^2] \right] \cdot \boldsymbol{\Pi} \quad (10c)$$

$$\triangleq \boldsymbol{\Omega}' \cdot \boldsymbol{\Pi} \quad (10d)$$

Equation 10a is a trivial rearrangement of Equation 9. In Equations 10b and 10c we manipulate terms in order to form matrices of the states multiplied by vectors of the parameters. Thus $[\dot{\boldsymbol{\omega}}]$ is a 3×6 matrix composed of elements that are functions of $\dot{\boldsymbol{\omega}}$, $[\boldsymbol{\omega}^2]$ is a 3×6 matrix filled with quadratic functions of $\boldsymbol{\omega}$, and $[\mathbf{q}^2]$ is a 3×3 matrix containing quadratic functions of the quaternions. The term $\{ \mathbf{I}_b \}$ is a vector of the six unique elements in the inertia matrix, and $\{ mg \mathbf{r}_g \}$ completes the parameter vector $\boldsymbol{\Pi}$ with the components of the center-of-gravity vector, as in Equation 1. It is clear from Equation 10b that the moments and products of inertia can be calculated given knowledge of the control torques, the angular velocities, and their derivatives. The mass and center of gravity are coupled and cannot be determined independently of one another; these terms are functions of the control torques and the attitude only.

The current sensor suite on the Whorl-I air bearing consists of three-axis rate gyros and linear accelerometers. The measurements from the linear accelerometers can be combined to provide a

single absolute vector measurement. With only one absolute measurement available, we expect the attitude estimate to suffer from drift; hardware to provide additional absolute measurements is under development. Moreover, this vector measurement is inherently noisy due to the derivative term required in its calculation, making it unusable at the present. The currently available vector of measurements with respect to the inertial lab frame is

$$\tilde{\mathbf{z}} = \boldsymbol{\omega}_b \quad (11)$$

The estimation techniques developed here are based on using $\tilde{\mathbf{z}}$ to determine $\hat{\mathbf{\Pi}}$.

A PRIORI ESTIMATES

We obtain initial estimates of the parameters through mass properties analysis of a CAD model. This model is of sufficient detail to include minor components but does not include the wiring harness. All commercial components are assumed to be uniform in density. Values obtained from the CAD model are shown in Table 1.

Table 1: Parameter Estimates From CAD Model

Parameter	Estimate
I_{xx}	6.2 kg·m ²
I_{xy}	-0.9 kg·m ²
I_{xz}	-0.8 kg·m ²
I_{yy}	7.5 kg·m ²
I_{yz}	0.2 kg·m ²
I_{zz}	12.1 kg·m ²
mg·r _{g_x}	-0.2 N·m
mg·r _{g_y}	-0.7 N·m
mg·r _{g_z}	-2.1 N·m

ALGORITHM DEVELOPMENT

One way to update the values obtained from a CAD model is through a least-squares estimation (LSE) algorithm. We investigate the basic requirements for effective use of an LSE method and develop several formulations for comparison. Fundamentally, LSE only implies use of some technique to find the best solution to an overdetermined problem in a least-squares sense. The development of the particular formulation of technique requires a working understanding of the physics of the system. In this section, we derive three different techniques for solving the parameter estimation problem within the context of LSE.

Torque Method

The progression from Equation 10d into the first least squares implementation requires only the definition of the pseudo-inverse. Using the definition of the matrix $\bar{\boldsymbol{\Omega}}'$, we solve Equation 10d via

$$\hat{\mathbf{\Pi}} = \left(\bar{\boldsymbol{\Omega}}'^T \bar{\boldsymbol{\Omega}}' \right)^{-1} \bar{\boldsymbol{\Omega}}'^T \bar{\mathbf{g}}_{rigidbody} \quad (12)$$

where the overbar notation indicates that the torque vector and state matrix are augmented by multiple sets of data. That is, $\bar{\boldsymbol{\Omega}}' = \left[\boldsymbol{\Omega}'^T|_{t_1}, \boldsymbol{\Omega}'^T|_{t_2}, \boldsymbol{\Omega}'^T|_{t_3}, \dots \right]^T$ and so too with the torque vector. Note that the $\boldsymbol{\Omega}'$ matrix must have more rows than columns for implementation of a regression technique, thus requiring the use of the pseudo-inverse equation as shown. This formulation is dubbed the torque method.⁷ Implementation requires application of a control torque to provide a persistent excitation to the system. The applied control must sufficiently excite every parameter in order for the algorithm to converge.

Recall that that matrix $\boldsymbol{\Omega}'$ contains functions of the states as well as the derivatives of the angular velocities. In an alternative formulation we integrate Equation 10d, leaving functions of the states and their integrals. The integrated form of the torque method is simply

$$\int_{t_0}^t \boldsymbol{\Omega}' \cdot \boldsymbol{\Pi} \, d\tau = \int_{t_0}^t \mathbf{g}_{rigidbody} \, d\tau \quad (13)$$

$$\boldsymbol{\Omega} \cdot \boldsymbol{\Pi} = \int_{t_0}^t \mathbf{g}_{rigidbody} \, d\tau \quad (14)$$

where the new matrix of states, $\boldsymbol{\Omega}$, contains functions of the angular velocities, quaternions, and their integrals — but no derivative terms. Motivation for this step is provided later in the paper.

The torque method is the most intuitive LSE formulation to derive. More refined LSE schemes for spacecraft parameter estimation make use of some of the special characteristics of the attitude dynamics associated with an orbiting spacecraft: the conservation of energy and the conservation of angular momentum. Before progressing to these techniques, however, we must expand this derivation to the gyostat equations.

Rewriting Equations 3 and 4 in terms of body and wheel angular velocities rather than angular momenta results in

$$\mathbf{I}_b \dot{\boldsymbol{\omega}}_b + \boldsymbol{\omega}_b^\times \mathbf{I}_b \boldsymbol{\omega}_b + mg \mathbf{r}_g^\times \mathbf{R}^{bi} \hat{\mathbf{k}} = \mathbf{A} \mathbf{I}_s \mathbf{A}^T \dot{\boldsymbol{\omega}}_s - \boldsymbol{\omega}_b^\times \mathbf{A} \mathbf{I}_s \boldsymbol{\omega}_s - \mathbf{A} \mathbf{g}_a + \mathbf{g}_{external} \quad (15)$$

where all of the terms on the right hand side are considered to be known. The left hand side is of the identical form to the rigid body equations, thus

$$\boldsymbol{\Omega}' \cdot \boldsymbol{\Pi} = \mathbf{A} \mathbf{I}_s \mathbf{A}^T \dot{\boldsymbol{\omega}}_s - \boldsymbol{\omega}_b^\times \mathbf{A} \mathbf{I}_s \boldsymbol{\omega}_s - \mathbf{A} \mathbf{g}_a + \mathbf{g}_{external} \quad (16)$$

Integrating both sides of the equation yields

$$\boldsymbol{\Omega} \cdot \boldsymbol{\Pi} = -\mathbf{A} \mathbf{I}_s \boldsymbol{\omega}_s - \int_{t_0}^t \boldsymbol{\omega}_b^\times \mathbf{A} \mathbf{I}_s \boldsymbol{\omega}_s \, d\tau + \int_{t_0}^t \mathbf{g}_{external} \, d\tau \quad (17)$$

Momentum Integral

An extension of the torque method LSE implementation is the momentum integral. In a space vehicle, this method makes use of the torque-free nature of the system such that for any pair of data points in time, t_1 and t_2 , the total angular momenta differ only by the rotation of the body in that time, \mathbf{R}^{21} . For proper modeling of the DSACSS system we retain the gravity gradient torque term, thus

$$\left(\boldsymbol{\Omega}' \cdot \boldsymbol{\Pi} - \mathbf{g}_{rigidbody} \right)_{t_2} = \mathbf{R}^{21} \left(\boldsymbol{\Omega}' \cdot \boldsymbol{\Pi} - \mathbf{g}_{rigidbody} \right)_{t_1} \quad (18)$$

$$\left(\boldsymbol{\Omega}' \Big|_{t_2} - \mathbf{R}^{21} \boldsymbol{\Omega}' \Big|_{t_1} \right) \cdot \boldsymbol{\Pi} = \mathbf{g}_{rigidbody} \Big|_{t_2} - \mathbf{R}^{21} \mathbf{g}_{rigidbody} \Big|_{t_1} \quad (19)$$

This formulation is clearly a time-lagged difference of the torque method, and as such can be integrated in exactly the same way. The length of the time lag is determined by the magnitude of

the shift: if t_2 and t_1 are subsequent data points, we term that a singly-shifted momentum integral technique. The momentum integral technique offers an advantage of additional smoothing of the data. Skipping one or more data points (doubly- or triply-shifting) can further smooth the data, but becomes unstable in the presence of unmodeled dissipation. Note that this technique halves the size of the data set, requiring a longer time span of data.

Energy Balance

The energy balance has been proposed as a more computationally efficient technique because it combines the three equations obtained at each time step into a single equation.^{6,7} This energy-like expression is obtained by dotting the angular velocity vector with the equations of motion of the system

$$\boldsymbol{\omega}_b^\top (\mathbf{I}_b \dot{\boldsymbol{\omega}}_b + \boldsymbol{\omega}_b^\times \mathbf{I}_b \boldsymbol{\omega}_b + mg \mathbf{r}_g^\times \mathbf{R}^{bi} \hat{\mathbf{k}}) = \boldsymbol{\omega}_b^\top (\mathbf{g}_{rigidbody}) \quad (20)$$

This transformation eliminates the rigid body contribution to the motion, because

$$\boldsymbol{\omega}_b^\top (\boldsymbol{\omega}_b^\times \mathbf{I}_b \boldsymbol{\omega}_b) = 0 \quad (21)$$

However, by only considering the motion in the direction of the angular velocity vector there is a risk of losing observability of one or more parameters.⁷

The integrated form of the energy balance equation is

$$\int_{t_0}^t \boldsymbol{\omega}_b^\top (\mathbf{I}_b \dot{\boldsymbol{\omega}}_b + mg \mathbf{r}_g^\times \mathbf{R}^{bi} \hat{\mathbf{k}}) d\tau = \int_{t_0}^t \boldsymbol{\omega}_b^\top (\mathbf{g}_{rigidbody}) d\tau \quad (22)$$

Note that the first term is the derivative of rotational kinetic energy

$$\boldsymbol{\omega}_b^\top \mathbf{I}_b \dot{\boldsymbol{\omega}}_b = \frac{1}{2} \boldsymbol{\omega}_b^\top \mathbf{I}_b \dot{\boldsymbol{\omega}}_b + \frac{1}{2} \dot{\boldsymbol{\omega}}_b^\top \mathbf{I}_b \boldsymbol{\omega}_b \quad (23)$$

$$= \dot{T}_r \quad (24)$$

and as such can be symbolically integrated to obtain

$$\boldsymbol{\omega}_b(t)^\top \mathbf{I}_b \boldsymbol{\omega}_b(t) - T_r(t_0) + \int_{t_0}^t \boldsymbol{\omega}_b^\top (mg \mathbf{r}_g^\times \mathbf{R}^{bi} \hat{\mathbf{k}}) d\tau = \int_{t_0}^t \boldsymbol{\omega}_b^\top (\mathbf{g}_{rigidbody}) d\tau \quad (25)$$

Unfortunately, there is no analog to the energy balance formulation for the gyrostat equations. Considering Equations 16 and 25 we can see a term involving the integration of $\dot{\boldsymbol{\omega}}_b$ and $\boldsymbol{\omega}_s$. It is not possible to evaluate this integral analytically. Numerical evaluation results in calculation of derivative terms, a step we are endeavoring to avoid. As such, we do not implement the energy balance technique in this investigation.

LEAST-SQUARES ESTIMATION PERFORMANCE

In the above section we developed three different LSE techniques. We have already discounted one of these techniques due to the requirement of calculating a numerical derivative. We justify this position below.

Several factors contribute to the convergence of the estimates. The control input must provide excitation of each parameter. Because we are relying on a simple numerical integration technique, step size plays a significant role in maintaining accurate numeric integration. Moreover, the dynamics of the system dictate the minimum step size for full observation. Simulation time determines the

size of the data set; however, longer simulation times lead to increased uncertainty levels due to the available sensor suite. Robustness to sensor noise is imperative. Note that noise can only impair the quality of an estimation: if a noise-free data set is degenerate in estimating one or more parameters, those parameters will not be accurately identified after the addition of random noise.

If any of the parameters are unobservable (or nearly so), $\mathbf{\Omega}^T \mathbf{\Omega}$ will have a corresponding number of singular values that approach zero. A singular value of exactly zero indicates a parameter that is not affecting the motion: such terms can be dropped from the solution set without loss of information. However, very small singular values may indicate only that a significant parameter is not being sufficiently excited, thus potentially leading to inaccurate estimation of the entire vector of parameters.

Natural vs. Integrated Forms

Batch estimation techniques compensate for random noise. However, the original matrix of states, $\mathbf{\Omega}'$, includes the derivatives of the angular velocity. Such terms must be computed numerically from the noisy rate gyro data; numerical derivatives, regardless of order, are highly unstable in the presence of noise. As such, running the LSE analysis by computing the natural form of the state matrix, as in Equations 16, 19, and 25 results in parameter estimates that are highly sensitive to the sensor noise. In contrast, the solution of the integrated form shown in Equation 17 requires that we compute numerical integrals rather than derivatives; numerical integration is robust to random noise.

We demonstrate this phenomenon in Figure 2. These plots present the performance of the natural (left plot) and integrated (right plot) forms of the torque method technique. We simulated a rigid body excited by a square wave thruster profile, firing about the z -axis only. The period of the square wave input, used as the ordinate axis for these plots, is representative of the excitation of the input. The level of simulated white, zero-mean, constant amplitude sensor noise defines the abscissa. The colormap axis presents the median percent-error of the nine-term parameter estimate. The parameter estimation problem is not particularly numerically well-conditioned: these physical values can easily span three orders of magnitude. This range of values does not cause problems in the numeric solution of the LSE, but it can make the results of the percent-error calculation unclear — the same absolute error in two parameters can yield very different percent error results. As such, the median value of the nine-term percent error vector provides a more consistent representation of algorithm performance than either the maximum value or the mean.

It is clear from the plots in Figure 2 that the integrated form of the equations is a much more stable formulation of the problem. High-frequency excitations are not observable due to the step size of the simulation; this Nyquist frequency cutoff is indicated by the label Ny on the ordinate axis. It is well-understood that these data will not produce valid estimates, regardless of sensor quality. However, once the system is maneuvering in an observable way, we expect that noisy sensor data could still be used to observe large-amplitude maneuvers, whereas higher-quality data should be able to produce good estimates from smaller motions. We see this behavior from the integrated techniques only. The natural form of the equations produces estimates only as good as the sensor data, regardless of the input signal: the convergence of the solution is driven by the quality of the numerical derivatives. Whereas the natural form only produces valid results with up to 1% sensor noise, the integrated form is shown to be robust to data with ten times that noise level. We expect up to 10% error from the experimental rate gyro data, thus the derivative representations are too sensitive to noise for this application. We continue considering only the integrated forms, and therefore only the torque method and momentum integral techniques.

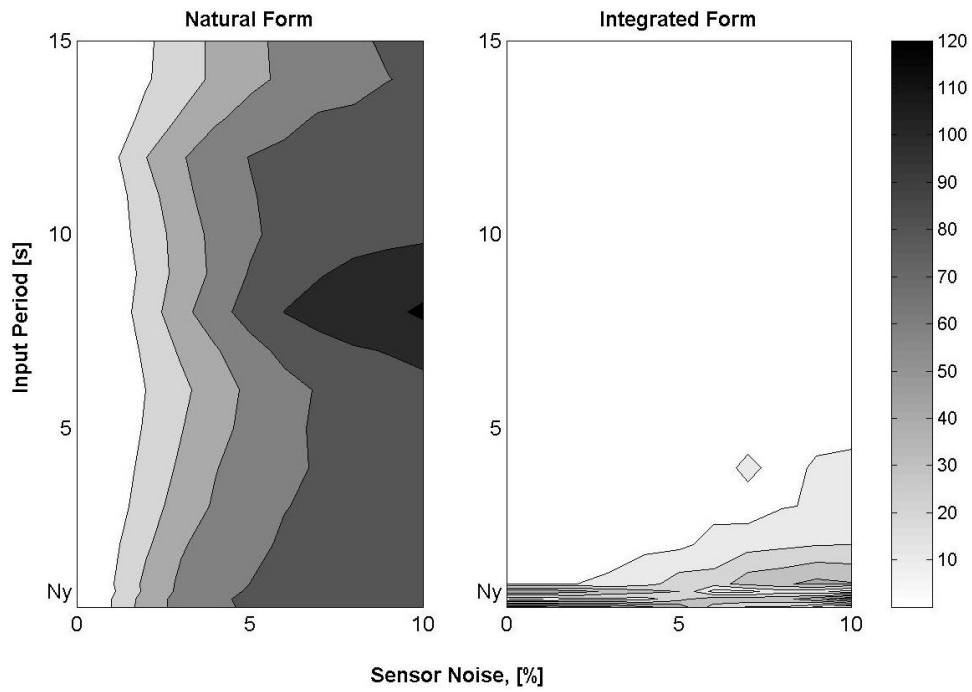


Figure 2: Torque Method LSE Performance in Natural and Integrated Forms [% Median Error]

Data Generation and Sample Performance

We now move to the full simulation of the Whorl-I gyrostat. Several levels of simulation are required in order to prepare for experimental investigation.

We begin with the simulation of a rigid body with simple mass properties controlled by thrusters. We select a basic torque profile, as the products of inertia and gravity gradient torque present in the physical system will provide additional excitation. This torque profile is presented in Figure 3. We use this torque profile largely because it provides a target momentum wheel history which we are largely able to duplicate experimentally; more information on this requirement is described later in the paper.

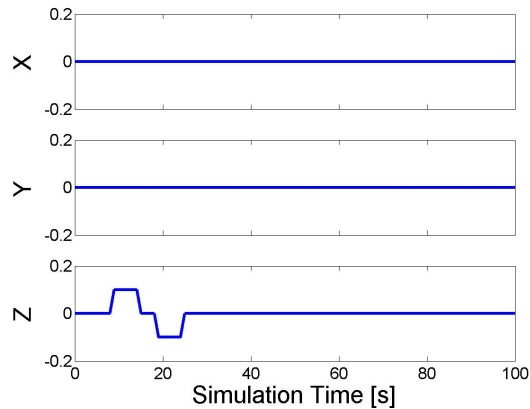


Figure 3: Simulation Thrust Profile [N]

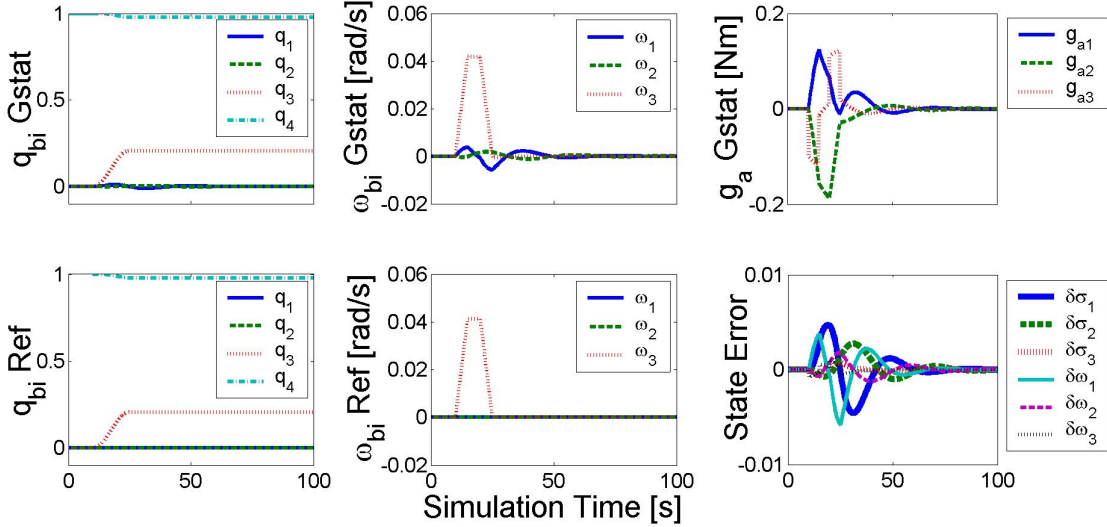


Figure 4: Data Generation / Tracking Controller Output

We use a nonlinear tracking control law originally derived for coupled thruster / momentum wheel control of a spacecraft.¹⁷ We simplify the first controller derived in this work by removing the thruster torques from the gyrostator system and compensating for them with the flywheels:

$$\begin{aligned} \mathbf{A} \mathbf{g}_a &= \mathbf{h}_b^\times \mathbf{J}^{-1} (\mathbf{h}_b - \mathbf{A} \mathbf{h}_a) + \mathbf{g}_g - \mathbf{J} \boldsymbol{\omega}_b^\times \delta \boldsymbol{\omega} \\ &\quad - \mathbf{J} \mathbf{R}^{br} \mathbf{I}_r^{-1} \mathbf{h}_r^\times \mathbf{I}_r^{-1} \mathbf{h}_r - \mathbf{J} \mathbf{R}^{br} \mathbf{I}_r^{-1} \mathbf{g}_g + k_1 \delta \boldsymbol{\omega} + k_2 \delta \boldsymbol{\sigma} \end{aligned} \quad (26)$$

where \mathbf{h}_r is the angular momentum of the reference rigid body, \mathbf{I}_r is the moment of inertia matrix of the reference body, \mathbf{R}^{br} is the rotation between the reference body frame and the gyrostator body frame, $\delta \boldsymbol{\omega}$ is the angular velocity error between the gyrostator and the reference body, and $\delta \boldsymbol{\sigma}$ is the attitude error in terms of Modified Rodrigues Parameters (MRPs). Note that we have also included the gravity gradient torque acting on the gyrostator, \mathbf{g}_g . This controller stabilizes the gyrostator system with the choice of any positive gains k_1 and k_2 .

The output of the simple simulation used to generate the desired experimental wheel speed profile is shown in Figure 4. The attitude and rate data for the reference body under thruster control are displayed below the same data for the simple gyrostator. The required motor torques are presented, as is the state error between the gyrostator and the reference body. Recall that the gyrostator in this simulation uses more simple mass properties than what we expect in the physical system. The more complex physical system will provide additional excitation of the parameters, not present in this simulation.

The above simulation provides a simple maneuver to attempt. However, we also require a simulation that will closely approximate the expected behavior of the physical system. We will use this data to draw conclusions about the experimental estimation. We use the best-guess mass properties listed in Table 1 to represent the experimental system and a step-size of $0.02s$, the mean loop time of the experimental system. We initially add no noise to the data in order to validate the performance of the algorithms. The percent error of each estimate for the noise-free case is shown in Table 2. Note that we use the torque method along with three momentum integral techniques. The shift magnitude for the momentum integral techniques is indicated by the parenthetical note in the table heading.

Table 2 shows that the parameters were well excited and therefore easily identified to great accuracy. This is as you would expect for the zero-noise case. Each of the techniques performs comparably;

Table 2: Performance with Perfect Simulated Data

Parameter	TM % Err	MI(1) % Err	MI(2) % Err	MI(3) % Err
I_{xx}	0.0939	-0.00157	0.0152	0.0866
I_{xy}	-1.15	0.0147	0.0112	-0.0259
I_{xz}	-0.444	0.00611	-0.00387	0.00418
I_{yy}	0.210	0.0479	0.0541	-0.0433
I_{yz}	4.14	0.0209	-0.0145	0.00386
I_{zz}	0.0582	0.00161	-0.0148	0.00870
$\text{mg}\cdot\mathbf{r}_{g_x}$	0.0467	0.000516	-0.000880	-0.00211
$\text{mg}\cdot\mathbf{r}_{g_y}$	0.434	-0.00468	-0.00499	-0.0106
$\text{mg}\cdot\mathbf{r}_{g_z}$	-0.133	0.000625	0.00171	0.00186

all error is due to the step-size of the first order numerical integration technique. Note that a negative percent error indicates that the estimated parameter is smaller than the expected value; although this is a non-traditional representation, we believe that this insight may prove valuable in interpreting experimental results.

In order to predict the realistic performance of the LSE algorithms we add artificial noise to the rate gyro data. We add white, zero-mean, constant magnitude noise based on the experimentally determined uncertainty. The quaternion values for the experimental system are obtained by numerically integrating the rate data, and as such are not noisy. The results of this simulation are shown in Table 3.

Table 3: Performance with Simulated 10% Noisy Rate Gyro Data

Parameter	TM % Err	MI(1) % Err	MI(2) % Err	MI(3) % Err
I_{xx}	-5.47	76.2	888.	15600.
I_{xy}	2290.	593.	5730.	88600.
I_{xz}	153.	72.3	1290.	22000.
I_{yy}	376.	-113.	538.	8732.
I_{yz}	2000.	384.	2430.	68000.
I_{zz}	-0.565	-5.46	0.401	238.
$\text{mg}\cdot\mathbf{r}_{g_x}$	-102.	-99.8	-98.9	-99.9
$\text{mg}\cdot\mathbf{r}_{g_y}$	-99.7	-99.6	-100.	-100.
$\text{mg}\cdot\mathbf{r}_{g_z}$	76.4	11.7	375.	24870.

Table 3 is a logical extension of the noise-free estimates. Although the MotionPak II is a high quality sensor, we are not making use of its full range in this experiment. The rate gyros have a sensing limit of $1.3\text{rad}/s$. At this range, an uncertainty of $\pm 0.0091\text{rad}/s$ is quite reasonable. However, the data we are working with has a maximum amplitude of $0.1\text{rad}/s$, resulting in a 10% error band. Parameters that are more difficult to estimate with perfect data are even more erroneous in the presence of noise. The singly-shifted momentum integral technique performs generally better than the torque method and the momentum integral techniques with larger time shifts. Despite the level of sensor noise, estimation of the I_{zz} and $\text{mg}\cdot\mathbf{r}_{g_z}$ terms, at a minimum, should be possible.

The experimental wheel speed signal has an uncertainty of only $\pm 0.4\%$. However, these values are calculated in real time by sampling the motor encoder for a pair of position measurements and calculating a first order derivative. This process is slow: we sample the rate gyros at an average rate of 41Hz but the wheel speed data is only updated at an average rate of 1.1Hz . As such, it is somewhat unclear as to what time the wheel speed data should actually be referenced. Specifically,

it seems likely that the wheel data is lagged by one step, slightly less than $1s$. We can correct for the shifting in the estimation routine; it is necessary to understand the effect of left- or right-shifting the wheel data with respect to the body data. We shifted the wheel data by up to $1.5s$, both left and right, holding all other data ideal (no noise added) for single-shift momentum integral analysis.

The behavior of the actual parameter estimates is shown in Figure 5. Note that this representation is a change from the percent error data presented earlier; it is useful for comparison to the experimental data later in the paper. It is obvious that small discrepancies in the time synchronicity of the data can result in high levels of error in the estimation. In the noise-free case, most inertia estimates go to a local extrema at the synchronized time. This behavior does not hold in the presence of noise, but Figure 6 provides an interesting insight. When the wheel data lags the body data the estimates of the parameters are erratic. However, the estimates follow a smooth trend from the synchronization point and with any data where the wheel data is ahead of the states. This pattern is used later to align the experimental data sets.

One final possible source of error in the system is the alignment of the wheel axes with respect to the rate gyro axes. We designed the system such that $\mathbf{A} \triangleq \mathbf{1}$, but it is unreasonable to assume that is the case. Unfortunately, it is not an uncertainty that can be easily quantified on the physical system. With the knowledge of manufacturing uncertainty and fit tolerances, we obtained an estimate of this error through manipulation of the CAD model. From this modeling, the MotionPak II could be rotated about the z -axis as much as 1.6° . We assume that the internal sensor array is square to the housing. Assuming the motors are perfectly aligned to the motor mounts and the flywheels are square to the motor shafts, the x - and y -flywheels could be rotated by as much as 2.0° about the z -axis. These individual errors yield a maximum relative alignment error for the x - and y -flywheels of 3.6° . With the additional assumption that the honeycomb deck is flat we can conclude that the z wheel must be perfectly aligned with the z rate gyro.

We can replicate this misalignment by rotating the simulated wheel speed data prior to LSE analysis. We make the (certainly false) simplifying assumption that the x - and y -flywheels are misaligned to the same degree. In the noise-free case, rotation error causes a linear change in the parameters; the sensitivity of each parameter to this error determines the slope of the line. The inclusion of rate gyro noise causes only an additional offset error at the nominal condition, as in Table 3.

EXPERIMENTAL RESULTS

All results presented up to this point have been from numerical simulations. This section details the performance of the same techniques as applied to data obtained from the Whorl-I platform, shown in Figure 8.

We quantified the experimental uncertainties in the preceding section. The one experimental quirk we did not discuss as yet is the performance of the motors. We cannot as yet accurately control the torque applied by the motors. As such, although we attempted to track the motion shown in Figure 4 there are substantial deviations. We believe the data itself to be accurate, however, and so accurate parameter estimation should still be possible.

The desired and actual trajectories for the body and wheel angular velocities are shown in Figure 8. Note that the raw rate gyro data are not shown here; in order to mitigate sensor noise, the data is smoothed through a moving average prior to analysis. The moving average dimension was selected to achieve a Nyquist frequency of ten times the natural frequency, $N_y = 10\nu$. The moving average provided a substantial improvement in data quality, reducing the standard deviation from 0.0080 to 0.0047 . As such, the smoothed rate gyro data has a 95% uncertainty of $\pm 0.0091 rad/s$. The wheel speed curves have an extremely long first mode, so we selected a moving average dimension corresponding to a Nyquist frequency 15 times greater than the natural frequency. The primary effect of wheel speed data preprocessing is to eliminate the stair-stepping effect and provide a continuous, smooth curve. The effects of smoothing are shown in Figure 9.

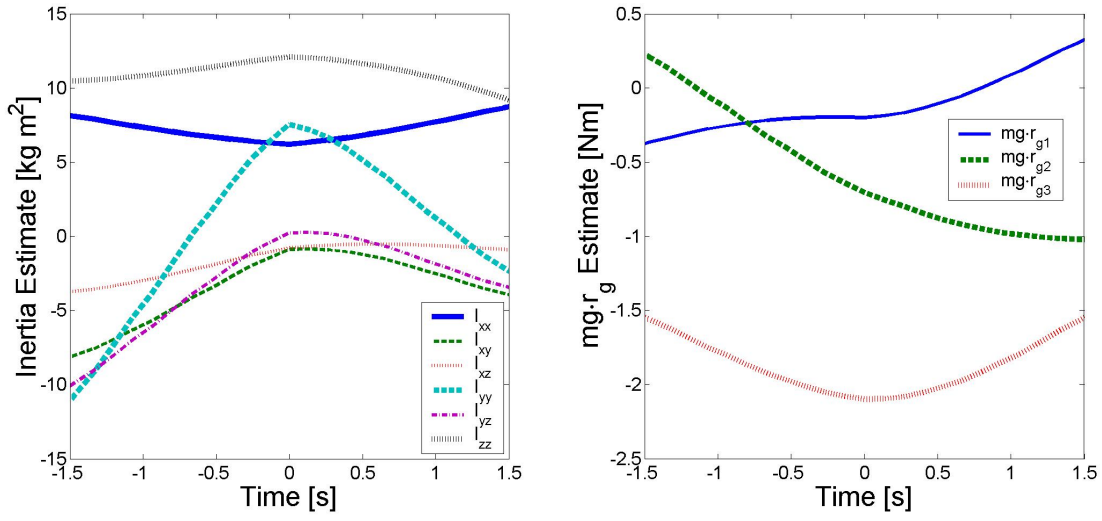


Figure 5: Effect of Time Synchronization, Perfect Data

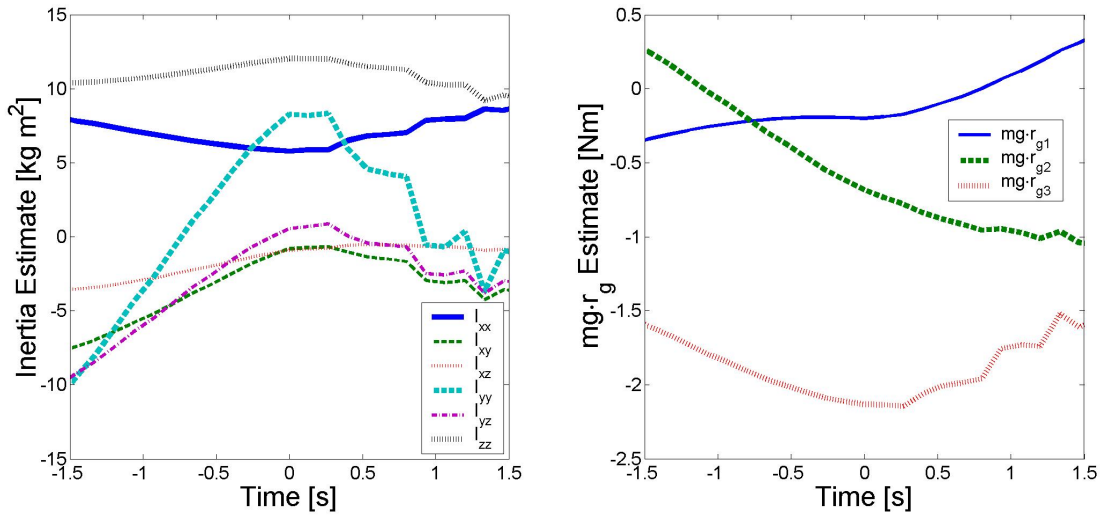


Figure 6: Effect of Time Synchronization, 10% Simulated Rate Gyro Noise

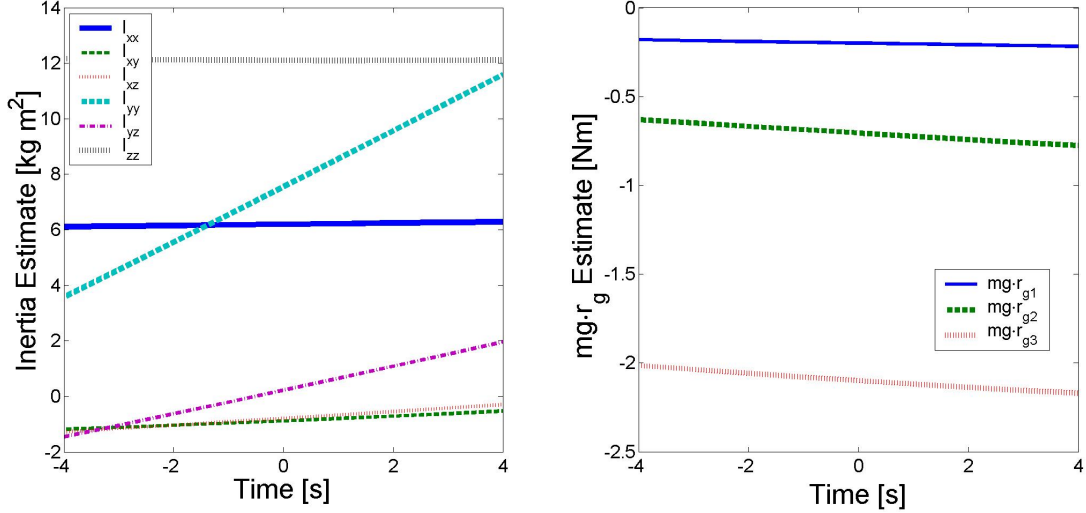


Figure 7: Effect of Angular Alignment, Perfect Data

We performed the same time-shift analysis on the experimental as we did with the simulated data. Recall that the trend indicated by Figure 6 suggested the existence of a break point when the wheel and state data are correctly synchronized. The experimental data shown in Figure 10 displays similar behavior, thus we conclude that the wheel data lags the state data by 7 data points, or $0.17s$. The direction of this result is as expected, although its magnitude is smaller than anticipated: qualitative analysis indicated a shift on the order of 30 points. All subsequent data is analyzed with this 7 point shift.

The effects of angular alignment, as shown in Figure 11, are more benign than expected. The very small slopes of the linear trends may be due to the simplifying assumption that the x and y flywheels are misaligned to the same extent. No improvement in estimation can be obtained from these results, but the apparent lack of dependency on the alignment matrix is encouraging.

The most likely estimates of the Whorl-I mass properties are shown in Table 4. None of the estimates are similar to the expected values. As such, it is difficult to have confidence in the estimates. It is encouraging that the principal inertias are all positive and the system is identified as a stable pendulum. However, the inertias are not all physically valid as some sets violate Sylvester's inequalities and the triangle inequalities. Further investigation is required.

Table 4: Most Likely Parameter Estimates from Experimental Data

Parameter	TM Est	MI(1) Est	MI(2) Est	MI(3) Est
I_{xx}	2.87	6.68	1.41	5.08
I_{xy}	0.817	1.08	-2.86	-0.101
I_{xz}	-13.0	-3.67	2.35	2.19
I_{yy}	1.83	2.80	3.50	1.83
I_{yz}	3.27	1.04	0.724	-2.08
I_{zz}	7.49	6.85	4.77	6.95
$mg \cdot r_{g_x}$	0.0127	0.0280	-0.0333	-0.00271
$mg \cdot r_{g_y}$	-0.0631	-0.0603	-0.0181	-0.0351
$mg \cdot r_{g_z}$	-6.60	-11.1	-7.29	-13.0

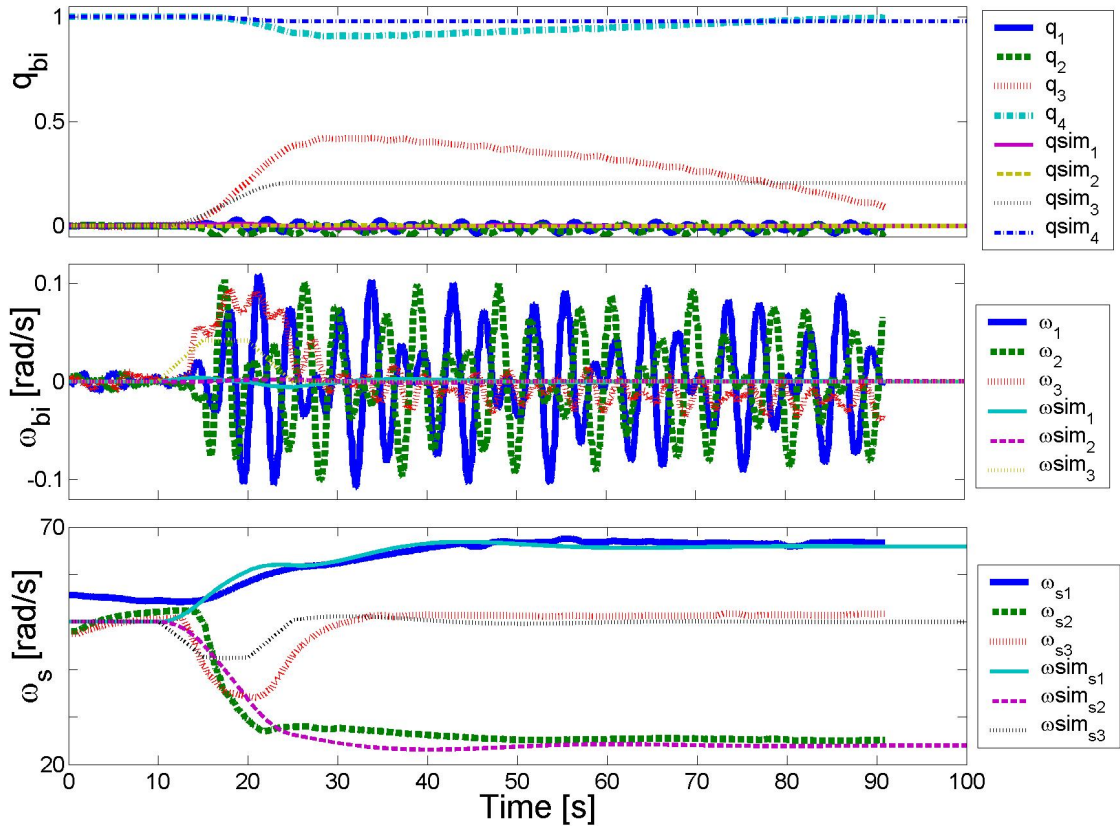


Figure 8: Data from Whorl-I Experiment

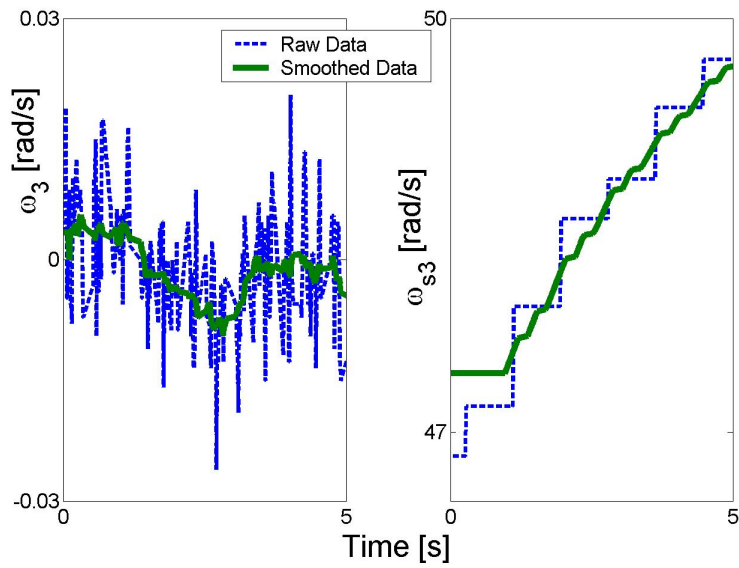


Figure 9: Smoothed Rate Gyro and Wheel Speed Data from Whorl-I Experiment

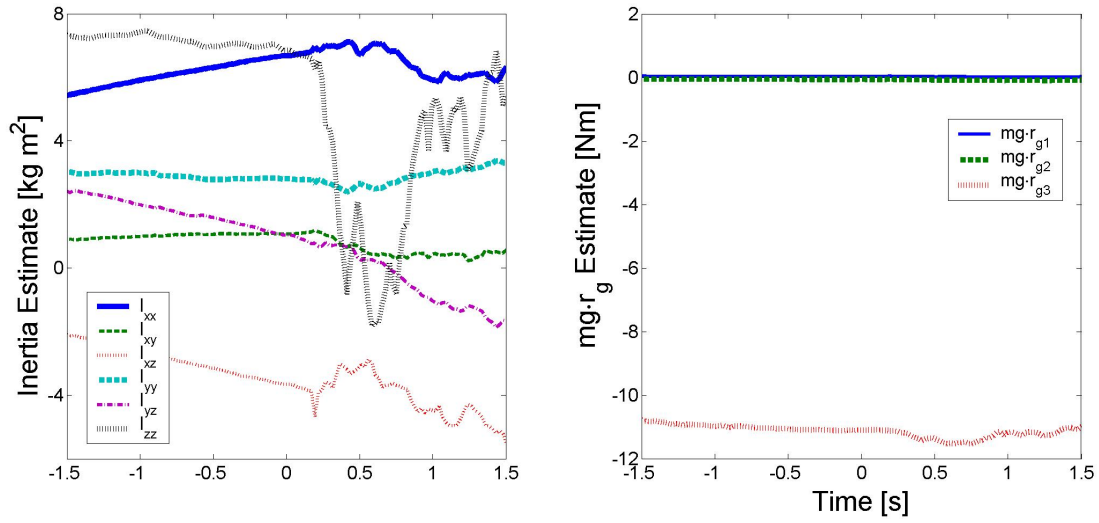


Figure 10: Investigation of Synchronization Time, Experimental Data

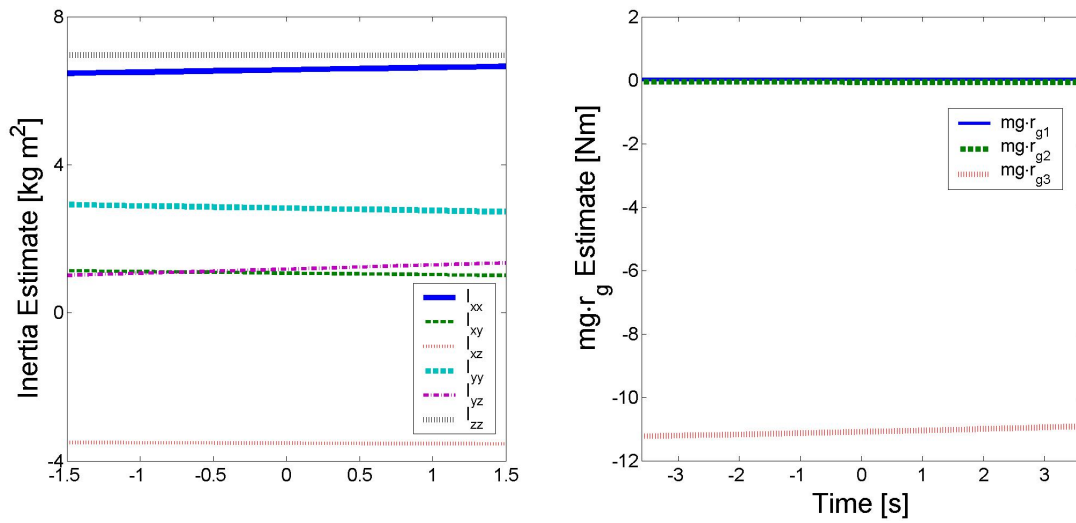


Figure 11: Investigation of Alignment Error, Experimental Data

CONCLUSIONS AND FUTURE WORK

In this paper we have proposed several techniques for the estimation of the mass properties of an air-bearing spacecraft simulator. We have developed these techniques and evaluated their performance in simulations of the physical system. Despite disappointing performance with experimental data, the techniques are valid. Performing a higher speed maneuver would allow the uncertainty of the rate gyro data to be less significant. The rate gyro noise appears to be the dominant source of error in this analysis.

We could endeavour to improve the estimation technique. There are many possibilities for variations on the batch techniques we have developed. We can enhance the realism of the model by means of a recursive optimization technique in which constraint equations are enforced.^{18,19} Modeling uncertainty through a Markov estimate rather than using LSE may also lead to improved convergence behavior.^{7,20} With improved attitude estimation, we could make use of a total least squares algorithm.¹¹ A recursive least squares algorithm could enforce Sylvester's inequalities and the triangle inequalities, preventing physically unrealizable solutions. Alternatively, we could invoke a recursive algorithm that attempts to minimize the difference between the estimated parameters and the best-guess of the parameters as obtained from the CAD model.⁸ More than likely, a nonlinear estimation scheme is required in order to also estimate the alignment matrix. This will require a substantial change in approach.

REFERENCES

- [1] B. Kim, E. Velenis, P. Kriengsiri, and P. Tsiotras, "A Spacecraft Simulator for Research and Education," in *Proceedings of the AIAA/AAS Astrodynamics Specialists Conference*, no. AAS 01-367, (Quebec City, Quebec, Canada), pp. 897–914, July 30–August 2, 2001.
- [2] G. S. Agnes and J. Fulton, "Design and Testing of SIMSAT — A Three-Axis Satellite Dynamics Simulator," in *Proceedings of the 42nd AIAA/ASME/ASCE/AHS/ASC Structures, Structural Dynamics, and Materials Conference and Exhibit*, no. AIAA 01-1591, (Seattle, Washington), April 16–19, 2001.
- [3] R. Thurber, "Dynamic Ground Simulation of Attitude Control Systems," in *Proceedings of the 35th AIAA Aerospace Sciences Meeting & Exhibit*, no. AIAA 97-0010, (Reno, Nevada), January 6–9, 1997.
- [4] V. J. Dabrowski and R. G. Cobb, "Experimental Demonstration of an Algorithm to Detect the Presence of a Parasitic Satellite," in *Proceedings of the AAS/AIAA Astrodynamics Specialists Conference*, no. AAS 03-610, (Big Sky, Montana), August 3–7, 2003.
- [5] M. G. Spencer, V. Chernesky, J. Baker, and M. Romano, "Bifocal Relay Mirror Experiments on the NPS Three Axis Spacecraft Simulator," in *Proceedings of the AIAA Guidance, Navigation, and Control Conference and Exhibit*, no. AIAA 02-5031, (Monterey, California), August 5–8, 2002.
- [6] S. Tanygin and T. Williams, "Mass Property Estimation Using Coasting Maneuvers," *Journal of Guidance, Control, and Dynamics*, vol. 20, no. 4, pp. 625–632, July–August 1997.
- [7] M. A. Peck, "Estimation of Inertia Parameters for Gyrostats Subject to Gravity-Gradient Torques," in *Proceedings of the AAS/AIAA Astrodynamics Specialist Conference*, no. AAS 01-308, (Quebec City, Quebec, Canada), July 30–August 2, 2001.
- [8] M. T. Carter, S. R. Vadali, and G. E. Chamitoff, "Parameter Identification for the International Space Station Using Nonlinear Momentum Management Control," in *Proceedings of the AIAA Guidance, Navigation, and Control Conference*, no. AIAA 97-3524, (New Orleans, Louisiana), pp. 252–262, August 11–13, 1997.

- [9] A. Y. Lee and J. A. Wertz, “In-Flight Estimation of the Cassini Spacecraft’s Inertia Tensor,” *Journal of Spacecraft and Rockets*, vol. 39, no. 1, pp. 153–154, January–February 2002.
- [10] C. Clemen, “New Method for On-Orbit-Determination of Parameters for Guidance, Navigation and Control,” *Acta Astronautica*, vol. 51, no. 1–9, pp. 457–465, July 2002.
- [11] M. L. Psiaki, “Estimation of the Parameters of a Spacecraft’s Attitude Dynamics Model Using Flight Data,” in *Goddard Space Flight Center Flight Mechanics Symposium*, no. 36, (Greenbelt, Maryland), October 28–30, 2003.
- [12] J. L. Schwartz and C. D. Hall, “Comparison of System Identification Techniques for a Spherical Air-Bearing Spacecraft Simulator,” in *Proceedings of the AAS/AIAA Astrodynamics Specialist Conference*, no. AAS 03-611, (Big Sky, Montana), August 3–7, 2003.
- [13] M. C. VanDyke, J. L. Schwartz, and C. D. Hall, “Unscented Kalman Filtering for Spacecraft Attitude State and Parameter Estimation,” in *Proceedings of the AAS/AIAA Space Flight Mechanics Conference*, no. AAS 04-115, (Maui, Hawaii), February 8–12, 2004.
- [14] J. L. Schwartz, M. A. Peck, and C. D. Hall, “Historical Survey of Air-Bearing Spacecraft Simulators,” *Journal of Guidance, Control, and Dynamics*, vol. 26, no. 4, pp. 513–522, July–August 2003.
- [15] A. J. Turner and C. D. Hall, “An Open Source, Extensible Spacecraft Simulation and Modeling Environment Framework,” in *Proceedings of the AAS/AIAA Astrodynamics Specialist Conference*, no. AAS 03-501, (Big Sky, Montana), August 3–7, 2003.
- [16] A. J. Turner, “An Open Source, Extensible Spacecraft Simulation and Modeling Environment Framework,” Master of Science, Virginia Polytechnic Institute and State University, Department of Aerospace and Ocean Engineering, Blacksburg, Virginia, July 2003.
- [17] C. D. Hall, P. Tsiotras, and H. Shen, “Tracking Rigid Body Motion Using Thrusters and Momentum Wheels,” *Journal of the Astronautical Sciences*, vol. 50, no. 3, pp. 311–323, 2002.
- [18] M. A. Peck, “Uncertainty Models for Physically Realizable Inertia Dyadics,” in *Goddard Space Flight Center Flight Mechanics Symposium*, no. 34, (Greenbelt, Maryland), October 28–30, 2003.
- [19] M. R. Akella, “Adaptive Control — A Departure from the Certainty-Equivalence Paradigm,” in *Proceedings of the John L. Junkins Astrodynamics Symposium*, no. AAS 03-279, (College Station, Texas), May 23–24, 2003.
- [20] P. Eykhoff, “Process Parameter and State Estimation,” *Automatica*, vol. 4, pp. 205–233, 1968.